Phase transitions in biogenic amorphous calcium carbonate

Yutao U. T. Gong[a], Christopher E. Killian[a,b], Ian C. Olson[a], Narayana P. Appathurai[c], Audra L. Amasino[a], Michael C. Martin[d], Liam J. Holt[b], Fred H. Wilt[b], and P. U. P. A. Gilbert[a,e,1,2]

[a]Department of Physics, University of Wisconsin-Madison, 1150 University Avenue, Madison, WI 53706; [b]Department of Molecular and Cell Biology, University of California, Berkeley, CA 94720; [c]Synchrotron Radiation Center, University of Wisconsin-Madison, Stoughton, WI 53589; [d]Advanced Light Source, Lawrence Berkeley National Laboratory, Berkeley, CA 94720; and [e]Department of Chemistry, University of Wisconsin-Madison, 1101 University Avenue, Madison, WI 53706

Edited by Alexandra Navrotsky, University of California, Davis, CA, and approved February 8, 2012 (received for review November 3, 2011)

Crystalline biominerals do not resemble faceted crystals. Current explanations for this property involve formation via amorphous phases. Using X-ray absorption near-edge structure (XANES) spectroscopy and photoelectron emission microscopy (PEEM), here we examine forming spicules in embryos of *Strongylocentrotus purpuratus* sea urchins, and observe a sequence of three mineral phases: hydrated amorphous calcium carbonate ($ACC \cdot H_2O$) → dehydrated amorphous calcium carbonate (ACC) → calcite. Unexpectedly, we find $ACC \cdot H_2O$-rich nanoparticles that persist after the surrounding mineral has dehydrated and crystallized. Protein matrix components occluded within the mineral must inhibit $ACC \cdot H_2O$ dehydration. We devised an in vitro, also using XANES-PEEM, assay to identify spicule proteins that may play a role in stabilizing various mineral phases, and found that the most abundant occluded matrix protein in the sea urchin spicules, SM50, stabilizes $ACC \cdot H_2O$ in vitro.

calcite | synchrotron | larva | echinoderm | echinodermata

Amorphous calcium carbonate (ACC) is an important precursor to geologic and biogenic calcium carbonate ($CaCO_3$) minerals, with natural and industrial relevance including CO_2 sequestration (1), scaling of pipes and desalination membranes (2), and biomineral formation (3). Within the last three years, important discoveries have revealed that $CaCO_3$ aggregates into particles up to 120 nm in size (4), and can grow faster than crystalline calcite (5). Synthetic ACC crystallizes readily, within minutes, particularly when it is in contact with water (6). In contrast, biogenic ACC persists for days in the animal, and months if extracted and stored dry (7).

Among the minerals formed by living organisms, or biominerals (8), the spicules formed by sea urchin larval embryos are widely studied because they are relatively simple biominerals, with 99.9 wt % calcite ($CaCO_3$) and 0.1 wt % proteins (9). In addition, with the publication of the sea urchin genome (10) and spicule proteome, many spicule proteins have been identified and isolated (11), although the functions of any of these proteins during spicule formation have not been identified. Sea urchin spicule mineralization initiates in the gastrula stage embryo (around 30 h postfertilization in *Strongylocentrotus purpuratus*) and takes place in a closed multicellular compartment termed a syncytium (12), with no space or water between the growing spicule mineral and the syncytial membrane (13). Spicule growth does not proceed atom by atom as in classical crystal growth from solution, but uses transient amorphous phases (7), with ACC first packed into 100-nm intracellular vesicles, and then delivered into the syncytial membrane (13). The use of ACC precursors elegantly circumvents the slow processes of crystal nucleation and growth from solution, whereas the exclusion of bulk water from the intracellular vesicles and from the syncytium prevents rapid ACC crystallization.

Sea urchin spicules were long suspected (14), and then confirmed (15, 16) to form via two ACC precursors, one hydrated and one not. Politi et al. (15) analyzed the surfaces of spicules and showed that there are indeed two amorphous mineral precursors in addition to calcite: a hydrated form of ACC, another distinct phase, that at the time was presumed to be anhydrous, and a crystalline calcite phase. These three surface phases, termed type 1 ($ACC \cdot H_2O$), type 2 (ACC), and type 3 (calcite), were observed to coexist and to crystallize with aging, but the precise sequence of transformation could not be identified directly (16). Later Radha et al. (6) showed that the enthalpy of transformation of fresh amorphous spicules, which contain approximately 50% type 2 ACC (14), is similar to the enthalpy of transformation from synthetic anhydrous ACC to crystalline calcite. Politi et al.'s interpretation of type 2 ACC as being anhydrous ACC in spicules, therefore, appeared likely to be correct.

Here we use X-ray absorption near-edge structure (XANES) spectroscopy combined with photoelectron emission spectromicroscopy (PEEM) with unprecedented spatial resolution, and show that in cross-sections of fresh spicules there are indeed the same three mineral phases identified by Politi et al. on spicule surfaces, and that the sequence of transformations is indeed $ACC \cdot H_2O \rightarrow ACC \rightarrow$ calcite, as proposed by Politi et al. (16) and by Radha et al. (6).

Previous studies with apparently contradictory observations have puzzled many scientists that worked on this system: Fresh, forming sea urchin spicules appear to contain amorphous calcium carbonate when observed by infrared spectroscopy (7) as well as when examined with X-ray absorption spectroscopy at the calcium K-edge (15), and L-edge (16). On the other hand, forming spicules appear to be crystalline calcite when examined using Raman microscopy (14), optical microscopy with crossed polarizers (17), and X-ray diffraction (18). In the latter case, the coexistence of an amorphous phase only appears (if at all) as a decrease in intensity of the crystalline peaks (7). How can the same material be simultaneously amorphous and crystalline, depending on the method used to observe it? It has long been suspected that crystalline and amorphous phases coexist, but direct evidence has been elusive. In the present study, XANES-PEEM experiments reconcile previous observations by showing that all phases, amorphous and crystalline, coexist at the nanoscale. Therefore, with the varying sensitivity and resolution of the different methods used previously, one mineral phase, or the other

Author contributions: P.U.P.A.G. designed research; Y.U.T.G., C.E.K., I.C.O., N.P.A., A.L.A., M.C.M., L.J.H., F.H.W., and P.U.P.A.G. performed research; C.E.K., N.P.A., M.C.M., L.J.H., and F.H.W. contributed new reagents/analytic tools; Y.U.T.G., A.L.A., and P.U.P.A.G. analyzed data; and Y.U.T.G., C.E.K., L.J.H., F.H.W., and P.U.P.A.G. wrote the paper.

The authors declare no conflict of interest.

This article is a PNAS Direct Submission.

Freely available online through the PNAS open access option.

[1]To whom correspondence should be addressed. E-mail: pupa@physics.wisc.edu.

[2]Previously published as Gelsomina De Stasio.

This article contains supporting information online at www.pnas.org/lookup/suppl/doi:10.1073/pnas.1118085109/-/DCSupplemental.

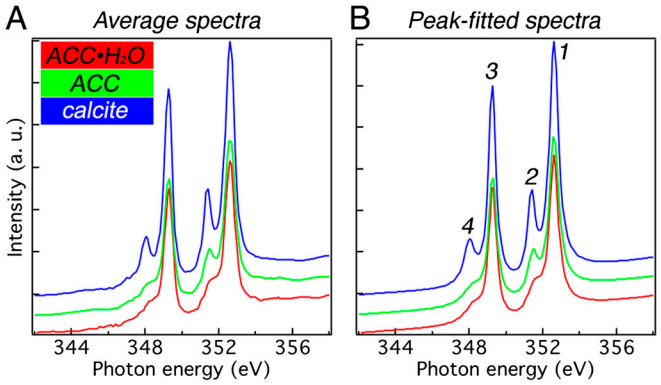

Fig. 1. The three reference spectra used for component analysis. (*A*) XANES spectra across the calcium L-edge extracted from sea urchin spicules. To minimize experimental noise, 6–10 independently acquired single-pixel spectra, with pixel sizes of 20 nm, were averaged to give each reference spectrum. (*B*) Spectra resulting from peak-fitting the spectra in *A*, which completely eliminates experimental noise from these spectra, thus they can be used as reference components for all analyses in this work. The red spectrum is hydrated amorphous calcium carbonate ($ACC \cdot H_2O$, see Fig. S1), the green spectrum is anhydrous ACC, and the blue spectrum is crystalline calcite, as identified by Politi et al. (16). A comparison of the three spectra highlights that the main peaks labeled 1 and 3 do not vary across the three mineral phases, whereas peaks 2 and 4 do vary. Specifically, in red $ACC \cdot H_2O$ both peaks are low, in green ACC peak 2 is high and peak 4 is low, whereas in calcite both are high. More details on how these spectra were obtained are provided in Fig. S2 and Table S1.

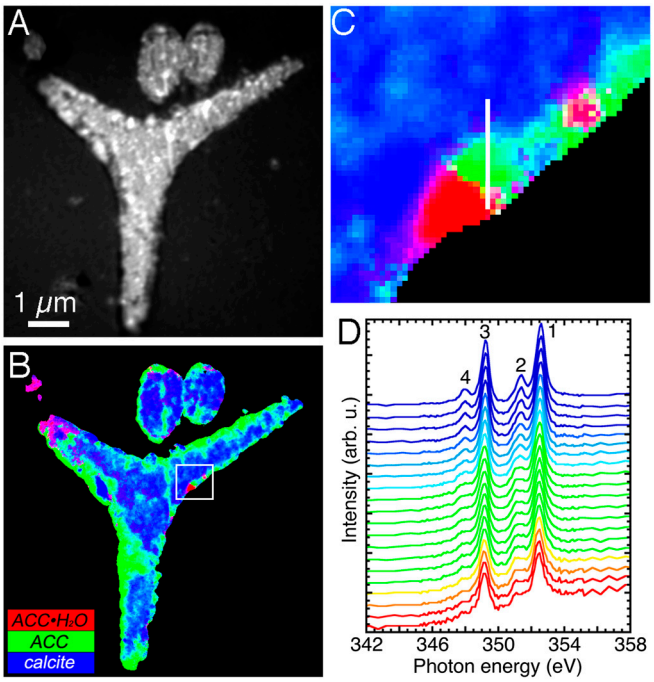

Fig. 2. Component mapping in 48-h spicules, at the prism developmental stage, analyzed within 24 h of extraction from the embryo. (*A*) XANES-PEEM image of three spicules embedded in epoxy, polished to expose a cross-section, and coated. The image is an average of all 121 images acquired across the Ca L-edge. The larger triradiate portion of a spicule at the center is polished in plane, whereas two other cylindrical spicules at the top have their long axes perpendicular to the plane of the image. (*B*) RGB map displaying the results of component mapping, in which each component is color-coded as in Fig. 1. The box indicates the region magnified in *C*. (*C*) Zoomed-in portion of the RGB map in *B*, where each 15-nm pixel shows a different color. Pure phases are R, G, or B, whereas mixed phases are cyan, magenta, or yellow, according to the rules of additive color mixing: G + B = C, R + B = M, R + G = Y (59). The white vertical line shows the positions of the 20 pixels from which the spectra in *D* were extracted. (*D*) Sequence of 20 XANES spectra extracted from 15-nm adjacent pixels along the white line in *C*. The color-coding is the same as used in *B*, *C*, and Fig. 1. Notice that the white line in *C* runs from the outer rim of the spicule (red), passing through orange, yellow, green, cyan, and finally blue, toward the crystalline center of the spicule. Correspondingly, moving from bottom to top across the spectra in *D*, one can see peak-2 growth leading, and peak-4 emergence and growth lagging.

prevails. Unexpected phase mixtures were detected, which led to the discovery of a unique protein function.

Results and Discussion

Mapping $CaCO_3$ Phases in Spicules. Sea urchin spicules were embedded in epoxy, polished to expose their cross-sections, and then coated as described in refs. 19 and 20. Once we identified a spicule with real-time PEEM imaging, we remained on the spicule and acquired stacks of images at varying photon energies, scanning across the calcium L-edge. Typical images had a 20-μm, or smaller, square field of view, and contained 10^6 pixels. Each pixel in a stack of images, therefore, had a size of 20 nm and contained a complete Ca XANES spectrum. With unique data processing software (21) we performed component analysis: We extracted a spectrum from each pixel and measured the proportion of each of the three component spectra shown in Fig. 1 (also see Figs. S1 and S2). The proportions were then displayed as colors in red, green, and blue (RGB) maps as the ones in Figs. 2 and 3 (also see Tables S1 and S2).

We analyzed a total of 83 spicule cross-sections, from three samples, and distinct embryo cultures, extracted 36 h, 48 h, and 72 h after fertilization, respectively, and found consistent results. Fig. 3 shows a representative set of spicules with different orientations, sizes, and developmental stages.

Several observations stand out from the transforming, 48-h spicules in Figs. 2 and 3. First, red pixels, which contain pure $ACC \cdot H_2O$, are usually localized at the periphery of the spicule, with few or none at the center. This finding is consistent with previous knowledge that new spicule mineral is deposited at the outer edges of the spicule (12, 13). One can conclude that the $ACC \cdot H_2O$ is short lived, and rapidly dehydrates after it is deposited on the spicule surface.

Dehydrated ACC green pixels are much more abundant than $ACC \cdot H_2O$ red pixels, and they too are preferentially localized all around the spicule outlines. Politi et al. (16) also used XANES-PEEM but were only able to analyze the surfaces of intact spicules, rather than cross-sections as presented here. They found that green ACC was the most abundant phase in forming spicules. Here we find 32% ACC in 48-h spicule cross-sections, whereas 72-h spicules do not show any residual green ACC in spicule cross-sections (Fig. 3, Table S2), which is consistent with previous Raman spectroscopy results (14).

Pure calcite blue pixels are concentrated at the center of the spicules. The sequence of spectra acquired going from the outside to the inside of the spicule cross-section (Fig. 2 *C* and *D*) shows the sequence of phase transformations, and their intermediates. This observation supplies direct evidence that the sequence of phase transformations leading to biogenic calcite is indeed $ACC \cdot H_2O \rightarrow ACC \rightarrow$ calcite. This sequence of transitions was hypothesized by Raz et al. (14) and Politi et al. (16) and then confirmed to be thermodynamically reasonable by Radha et al. (6). Our studies here directly observe these transitions in time and space in biogenic minerals.

We observe few yellow pixels ($Y = R + G = ACC \cdot H_2O +$ ACC), which is consistent with the paucity of red $ACC \cdot H_2O$ observed, and its short lifetime. There are, however, numerous cyan pixels ($C = G + B = ACC +$ calcite) indicating that ACC in those pixels is transforming to crystalline calcite; but there are also abundant magenta pixels ($M = R + B = ACC \cdot H_2O +$ calcite, Fig. S3) even at the center of the spicules, where most of the mineral is already crystalline. This final observation

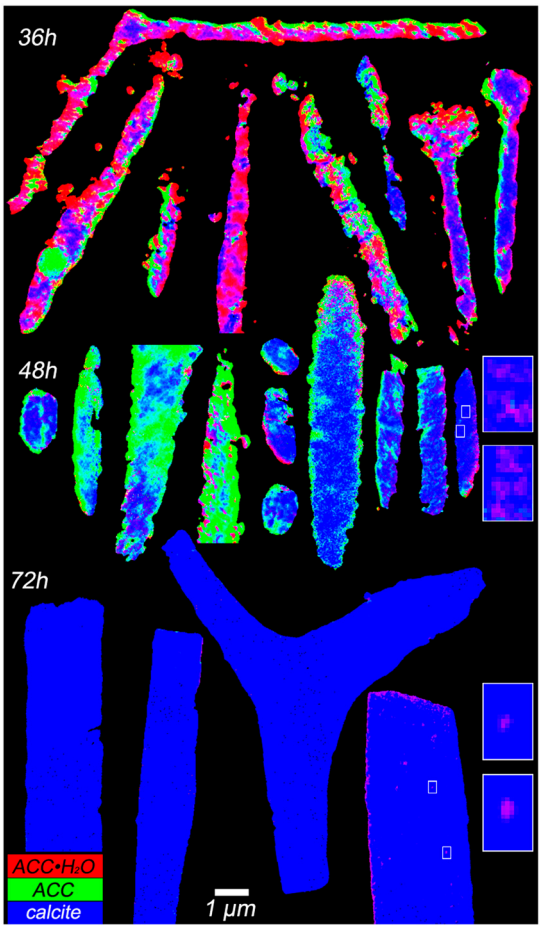

Fig. 3. RGB maps resulting from component analysis done on spicules extracted 36 h, 48 h, and 72 h after fertilization, analyzed within 24 h of extraction from the embryos. Horizontally, the spicules are ordered from most amorphous to most crystalline. Notice the large density of R and B pixels in 36-h, and 72-h spicules, respectively. See Table S2 for a quantitative analysis of R, G, B pixels. In the 48-h spicules R and G pixels, indicating amorphous phases, are always at the outer rims, whereas blue crystalline calcite is always at the center of each cross-section. Also notice that magenta nanoparticles are quite frequent (see spicules on the right, for instance). Magenta nanoparticles are made of colocalized ACC · H_2O and calcite. *Insets* on the right show zoomed-in maps of the four regions in white boxes on the 48-h and 72-h spicules on the right. (*Insets*) Pixels are 20 nm, and the color balance has been adjusted to enhance the magenta nanoparticle, otherwise faint, because magenta nanoparticles contain a much greater proportion of calcite than ACC · H_2O. These nanoparticles are 60–120 nm in size, and are consistently surrounded by blue calcite. See Fig. S3 for further spectroscopic analysis of the magenta nanoparticles.

was unexpected and led us to investigate how the short-lived ACC · H_2O persists in this way.

In Fig. S4 we present additional infrared data showing that spicules become progressively dehydrated as the embryo develops from 48 to 72 h (prism to pluteus stages), and the mineral crystallizes. Each infrared spectrum is strongly averaged over many spicules, and hence has significance for the chemical composition of spicules. The spatial distributions of Figs. 2 and 3 are in agreement with the infrared result, but provide much greater resolution. Notice in particular that in transforming spicules at 48 h the center of the spicules in cross-section is mostly crystalline, whereas amorphous phases tend to be localized at the outer rims.

The Persistence of ACC · H_2O. Given the ACC · H_2O → ACC → calcite sequence of phase transitions established in Fig. 2, it is surprising that we find magenta nanoparticles of ACC · H_2O + calcite in the middle of the spicule cross-sections surrounded by blue calcite and not by green dehydrated ACC (Figs. 2 and 3). The magenta nanoparticles persist 2 mo after extraction from the embryo, as shown in Fig. S5. We hypothesize that there is an inhibiting agent that greatly delays or completely stops the transition from ACC · H_2O → ACC. This inhibitor is likely a protein or proteins because nucleic acids, lipids, and polysaccharides are not found in the spicule (22). We propose that when the inhibitory proteins are trapped in specific locations inside a crystallizing spicule, the ACC · H_2O in those locations cannot dehydrate.

Radha et al. (6) showed recently that both transitions ACC · H_2O → ACC and ACC → calcite have negative enthalpies of transformation. These transitions are energetically favorable and should happen spontaneously with time in the absence of inhibitory molecules. However, the persistence of ACC · H_2O in the magenta nanoparticles suggests that occasionally there is a high activation barrier for the ACC · H_2O → ACC transition perhaps because of proteins that inhibit this transition, thus stabilizing ACC · H_2O. Aizenberg et al. (23, 24) showed a similar function of polyanionic proteins in mollusk shells that stabilize ACC.

Our model simulation shows how the presence of dehydration-inhibiting protein(s) results in islands of ACC · H_2O after crystallization of the spicule (Fig. S6 and Movies S1 and S2). Crystallinity propagates through the fully formed, space-filling (25), three-dimensional anhydrous amorphous phase, following random-walk patterns in three dimensions. This mechanism was first described by Killian et al. (26) in the polycrystalline matrix of the sea urchin tooth, and we believe that it occurs identically in the sea urchin spicules studied here.

Persisting, long-lived nanoparticles of dehydrated ACC (green or cyan) are not found anywhere in spicule cross-sections. This result suggests that the dehydration and crystallization transitions have very different dynamics. These transitions happen in minutes in synthetic ACC, but much more slowly in spicules: Green and red pixels persist 24 h after extraction from the embryo (Figs. 2 and 3–48 h). Both transitions, therefore, must be inhibited in vivo.

In Fig. 3, compared to the newly formed 36-h, and the almost entirely crystalline 72-h, the transforming 48-h spicules are the most revealing to analyze and discuss in depth. Based on the spicules in Fig. 3, and the following considerations, we arrived at a schematic representation of the energy landscape of the ACC · H_2O → ACC → calcite transitions, and the hypothetical activation barriers between them, as presented in Fig. S7. First, the transitions from red to green (dehydration) and from green to blue (crystallization) are thermodynamically downhill (exothermic) (6). Second, the majority of ACC · H_2O is short-lived, as is evident from its paucity in 48-h spicules in Figs. 2 and 3–48 h, and its restriction to the zone of deposition at the outer rims of the spicules in transforming 48-h spicules. The dehydration transition, therefore, must be fast, and correspondingly the activation barrier for ACC · H_2O → ACC must be the smallest. Third, in 48-h spicules there are many more green pixels than there are red pixels (Figs. 2 and 3–48 h). In addition, in 48-h spicules analyzed 4 d after extraction, some green ACC is still detectable (see Fig. S5), therefore the activation barrier for ACC → calcite must be greater than that for ACC · H_2O → ACC. Fourth, in the presence of inhibiting protein(s), the activation barrier becomes much larger, because even 2 mo after extraction the ACC · H_2O in those magenta nanoparticles still had not dehydrated nor crystallized (see Fig. S5).

The Role of SM50 in Stabilizing ACC · H_2O. We devised an assay to identify proteins that stabilize amorphous calcium carbonate mineral forms in vitro. A promising candidate is the sea urchin matrix protein SM50. SM50 is the most prevalent integral matrix protein from sea urchin embryonic spicules, as well as from adult

spines, tests, and teeth (11, 27, 28). An incorrect amino acid sequence for SM50 was originally published in 1987 at the time of the report of the initial cloning of the SM50 gene and its cognate complementary DNA (29, 30). The corrected SM50 amino acid sequence was published in 1991 (31). The SM50 protein is neither glycosylated (32) nor phosphorylated (11, 32), and it has an alkaline pI (31, 32). In fact, SM50 is one of the most alkaline of the spicule matrix proteins (32). Previous studies have also shown that decreasing SM50 protein levels in sea urchin embryos causes spiculogenesis to stop (17, 33). The *Lytechinus pictus* sea urchin ortholog of SM50, designated LSM34, has also been shown to directly interact with mineralizing calcium carbonate (34).

Fig. 4 and Fig. S8 show the spectroscopic results of the in vitro assays for the proteins stabilizing amorphous mineral phases. In this assay, a water droplet dissolves the topmost layers of geologic calcite. If the droplet deposited is just water, then as the droplet dries and the water evaporates, the ion clusters recrystallize as calcite. If, instead, the inhibiting protein is present in the droplet solution, it prevents dehydration and crystallization, thereby making ACC · H_2O the spectroscopically detectable species in the dried droplet.

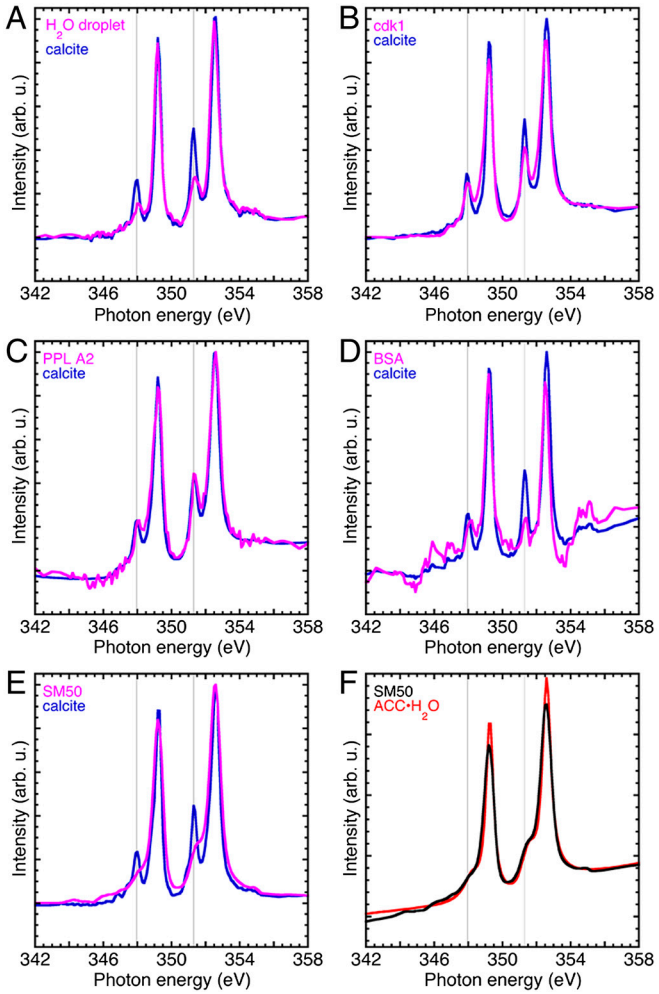

Fig. 4. Ca L-edge spectra acquired with XANES-PEEM on the surface of single-crystal calcite wafers, after depositing a droplet of water or protein in water, and letting it air dry. All data were acquired at the edge of each dried droplet, thus the two spectra in each plot were acquired simultaneously (magenta and blue curves). (*A*) The water droplet suspends a few ions or ion clusters, which then reprecipitate as calcite. The lower intensity crystal field peaks (vertical lines) in the H_2O-dried droplet spectrum indicate a polycrystalline calcite precipitate. (*B*) Cdk1 is a yeast cell cycle kinase expressed and extracted with the same methods used for SM50. This control spectrum also shows calcite reprecipitation. (*C*) PPL A2 is another protein present in sea urchin spicules (11). (*D*) The BSA dried droplet was very thick, hence the Ca signal is weak and noisy, but clearly calcite. (*E*) In the presence of the spicule matrix protein SM50 the reprecipitate is not calcite but hydrated ACC. (*F*) The SM50 spectrum from *E*, overlapped with the fitted ACC · H_2O from Fig. 1*B* (red curve). The two spectra are very similar. Hence we deduce that SM50 stabilizes ACC · H_2O, even in a dried droplet, in ultra-high vacuum, and in direct contact with a crystalline calcite wafer.

We tested SM50 because it is a very prevalent spicule matrix protein. Phospholipase A2 (PPL A2) and cyclin-dependent kinase 1 (cdk1) proteins were tested as controls. PPL A2 from honeybees was used because there is a PPL A2 present in the sea urchin spicule matrix (11). Cdk1 was tested as a control isolated from yeast using the same procedure as the SM50 protein, and because there is no cdk1 in the spicule matrix. This control ensures that the spectroscopic results were not an artifact of the protein preparation. BSA was used as another, non-sea-urchin, non-yeast-prepared control protein.

In Fig. S9 we present Ca and C spectra from all the proteins assayed, confirming that XANES spectroscopy is not simply detecting Ca, but Ca in a cluster of $CaCO_3$ extending at least to the nearest neighboring O atoms in all samples. Only areas of droplet that exhibited both carbonate crystal field peaks in Ca spectra and carbonate π^* peak at 290.3 eV in C spectra were accepted. The latter is a sharp, intense peak distinct from all other peaks in any organic or mineral C-containing species (35). It is impossible that the spectra we interpret as ACC · H_2O are instead single Ca^{2+} ions, each associated with one protein, because these would not show crystal field peaks in Ca spectra, nor a carbonate peak in C spectra, whereas all data presented show both.

The spectra in Fig. 4 show clearly that SM50 stabilizes ACC · H_2O in vitro whereas the other control proteins do not. These findings suggest that SM50 may stabilize ACC · H_2O in sea urchin-mineralized tissues. Because as many as 218 different proteins have been identified in the spicule (11), it is likely that other proteins along with SM50 stabilize ACC · H_2O. SM50 has been found to localize at the outer rim of the spicule (36, 37), where ACC · H_2O stabilization is most important, placing SM50 at the appropriate location in the spicule for it to function as an ACC · H_2O-stabilizing factor. Seto et al. (36), Urry et al. (37), and Killian and Wilt (32) have also detected SM50 occluded at lower density inside the spicule, which is where we observe the magenta nanoparticles. All these observations support the possibility that SM50 stabilizes ACC · H_2O in vivo. SM50 was first cloned 25 years ago (29). However, only in the context of our recent understanding of the dynamics of the mineral phase transformations in sea urchin spicules, and with the advent of powerful spectroscopic and molecular tools, are we now able to decipher SM50's possible function.

Understanding the specific mechanism by which SM50 may stabilize ACC · H_2O is the next challenge. Acidic proteins have long been suspected to play a major role in carbonate biomineralization, and there is much evidence that such proteins stabilize ACC · H_2O (14, 23, 24, 38). SM50, however, is not an acidic protein (31, 32).

The function of only a few biomineral proteins has been identified thus far. Suzuki et al. (39) isolated a protein called Pif that is essential for mollusk shell nacre formation. Starmaker is a protein expressed in zebrafish, which Nicolson and coworkers (40) have shown to be necessary for aragonite polymorph selection, and morphology in the zebrafish otolith. Notwithstanding this paucity of functional analyses, amorphous mineral phases are widespread in biominerals. Therefore the role of proteins acting as inhibitors of phase transition is probably not restricted to sea urchin spicules. Amorphous mineral phases have been identified in forming biominerals from different phyla: echinoderms (7, 16, 26, 41), mollusks (42–44), crustaceans (38, 45–51), annelids (52–54), porifera (55), urochordates (24, 56), and chordates (57, 58). Therefore, the phase transitions and their regulation by

organic molecules observed here may be shared by numerous $CaCO_3$-mineralizing organisms. Biomineralization is a major mechanism of carbon sequestration and therefore a better understanding of this process is of major biogeochemical, environmental, and economic importance.

Methods

Detailed methods are described in *SI Methods*. Sea urchin spicules from 36 h, 48 h, and 72 h embryos were extracted, embedded in epoxy, polished to expose spicule cross-sections, coated with 1-nm Pt in the area to be analyzed by XANES-PEEM, and 40-nm Pt around it (19). They were then analyzed with PEEM-3 on beamline 11.0.1 at the Berkeley-Advanced Light Source. A stack of images was collected across the Ca L-edge, between 340 and 360 eV photon energy (121 images, with field of view either 15×15 μm or 20×20 μm images, 10^6 pixels per image, and pixel sizes 15-nm or 20-nm, respectively), with a sample voltage of −15 kV. Each pixel in a stack contained the complete Ca XANES spectrum, and was fit to a linear combination of the three component spectra in Fig. 1, with proportions of the three components as the fit parameters. The resulting three numbers per pixel were then displayed as RGB maps in Adobe Photoshop, so that pure phases appear red, green, or blue, and mixed phases have intermediate colors, according to additive color mixing rules (59). Each spicule was analyzed in duplicate or triplicate, with reproducible results. Radiation damage, as described in Fig. S10, was prevented by keeping exposure times short.

The assay to test protein functions in vitro was done by depositing 1-μL droplets of 0.1 μg/μL protein solution on the surface of calcite wafers. Control droplets contained only water. Once the droplet had air-dried, the calcite wafer was inserted into ultra-high vacuum (10^{-10} Torr) and analyzed with SPHINX (60) (also a XANES-PEEM) at the Synchrotron Radiation Center. Ca and C spectra from the dried droplet and the surrounding calcite were analyzed simultaneously, and compared. Only areas of droplets that exhibited carbonate features in both Ca and C spectra were accepted. Water and all single proteins except for SM50 reprecipitated calcite, spicule matrix proteins reprecipitated ACC as expected (14), whereas SM50 reprecipitated ACC · H_2O.

ACKNOWLEDGMENTS. We thank Benjamin Gilbert for developing the Gilbert Group Macros (GG-Macros), Andreas Scholl, Anthony Young, and Andrew Doran for their assistance during the experiments on PEEM-3 at the Advanced Light Source (ALS), and Howard Padmore and Richard Celestre for their support in setting up a sample preparation laboratory, enabling fresh spicules to be prepared near the ALS. We thank Elia Beniash and Adam F. Wallace for discussions, and Lia Addadi and Steve Weiner for their valuable criticism of the manuscript. This work was supported by Department of Energy (DOE) Award DE-FG02-07ER15899, National Science Foundation (NSF) Awards CHE-0613972 and DMR-1105167, and University of Wisconsin-Hamel Award (to P.U.P.A.G.). L.J.H. is supported by a Bowes Research Fellows Award. The experiments on spicules were performed at the Berkeley-Advanced Light Source, supported by DOE under contract DE-AC02-05CH11231, those on proteins were done at the Synchrotron Radiation Center, which is funded by NSF Award DMR-0537588, and the University of Wisconsin-Madison and operated by the Graduate School of the University of Wisconsin-Madison.

1. Lackner KS (2003) A guide to CO_2 sequestration. *Science* 300:1677–1678.
2. Sheikholeslami R (2003) Mixed salts—scaling limits and propensity. *Desalination* 154:117–127.
3. Weiner S, Sagi I, Addadi L (2005) Choosing the crystallization path less traveled. *Science* 309:1027–1028.
4. Pouget EM, et al. (2009) The initial stages of template-controlled CaCO(3) formation revealed by cryo-TEM. *Science* 323:1455–1458.
5. Raiteri P, Gale JD (2010) Water is the key to nonclassical nucleation of amorphous calcium carbonate. *J Am Chem Soc* 132:17623–17634.
6. Radha AV, Forbes TZ, Killian CE, Gilbert PUPA, Navrotsky A (2010) Transformation and crystallization energetics of synthetic and biogenic amorphous calcium carbonate. *Proc Natl Acad Sci USA* 107:16438–16443.
7. Beniash E, Aizenberg J, Addadi L, Weiner S (1997) Amorphous calcium carbonate transforms into calcite during sea urchin larval spicule growth. *Proc R Soc Lond B Biol Sci* 264:461–465.
8. Lowenstam HA, Weiner S (1989) *On Biomineralization* (Oxford Univ Press, Oxford) p 324.
9. Wilt F (1999) Matrix and minerals in the sea urchin larval skeleton. *J Struct Biol* 126:216–226.
10. Consortium SUGS, et al. (2006) The genome of the sea urchin *Strongylocentrotus purpuratus*. *Science* 314:941–952.
11. Mann K, Wilt FH, Poustka A (2010) Proteomic analysis of sea urchin (*Strongylocentrotus purpuratus*) spicule matrix. *Proteome Sci* 8:33.
12. Wilt FH (2002) Biomineralization of the spicules of sea urchin embryos. *Zool Sci* 19:253–261.
13. Beniash E, Addadi L, Weiner S (1999) Cellular control over spicule formation in sea urchin embryos: A structural approach. *J Struct Biol* 125:50–62.
14. Raz S, Hamilton PC, Wilt FH, Weiner S, Addadi L (2003) The transient phase of amorphous calcium carbonate in sea urchin larval spicules: The involvement of proteins and magnesium ion in its formation and stabilization. *Adv Funct Mater* 13:480–486.
15. Politi Y, et al. (2006) Structural characterization of the transient amorphous calcium carbonate precursor phase in sea urchin embryos. *Adv Funct Mater* 16:1289–1298.
16. Politi Y, et al. (2008) Transformation mechanism of amorphous calcium carbonate into calcite in the sea urchin larval spicule. *Proc Natl Acad Sci USA* 105:17362–17366.
17. Wilt FH, Croker L, Killian CE, McDonald K (2008) The role of LSM34/SpSM50 in endoskeletal spicule formation in sea urchin embryos. *Invert Biol* 127:452–459.
18. Berman A, et al. (1993) Biological-control of crystal texture—a widespread strategy for adapting crystal properties to function. *Science* 259:776–779.
19. De Stasio G, Frazer BH, Gilbert B, Richter KL, Valley JW (2003) Compensation of charging in X-PEEM: A successful test on mineral inclusions in 4.4 Ga old zircon. *Ultramicroscopy* 98:57–62.
20. Gilbert PUPA, Frazer BH, Abrecht M (2005) The organic-mineral interface in biominerals. *Molecular Geomicrobiology*, Reviews in Mineralogy and Geochemistry, eds JF Banfield, KH Nealson, and J Cervini-Silva (Mineralogical Society of America, Washington, DC), Vol 59, pp 157–185.
21. GG-Macros., http://home.physics.wisc.edu/gilbert/.
22. Benson SC, Benson NC, Wilt F (1986) The organic matrix of the skeletal spicule of sea-urchin embryos. *J Cell Biol* 102:1878–1886.
23. Aizenberg J, Lambert G, Addadi L, Weiner S (1996) Stabilization of amorphous calcium carbonate by specialized macromolecules in biological and synthetic precipitates. *Adv Mater* 8:222–226.
24. Aizenberg J, Lambert G, Weiner S, Addadi L (2002) Factors involved in the formation of amorphous and crystalline calcium carbonate: A study of an ascidian skeleton. *J Am Chem Soc* 124:32–39.
25. Yang L, Killian CE, Kunz M, Tamura N, Gilbert PUPA (2011) Biomineral nanoparticles are space-filling. *Nanoscale* 3:603–609.
26. Killian CE, et al. (2009) The mechanism of calcite co-orientation in the sea urchin tooth. *J Am Chem Soc* 131:18404–18409.
27. Mann K, Poustka AJ, Mann M (2008) In-depth, high-accuracy proteomics of sea urchin tooth organic matrix. *Proteome Sci* 6:33.
28. Mann K, Poustka AJ, Mann M (2008) The sea urchin (*Strongylocentrotus purpuratus*) test and spine proteomes. *Proteome Sci* 6:22.
29. Benson S, Sucov H, Stephens L, Davidson E, Wilt F (1987) A lineage-specific gene encoding a major matrix protein of the sea-urchin embryo spicule. I. Authentication of the cloned gene and its developmental expression. *Dev Biol* 120:499–506.
30. Sucov H, et al. (1987) A lineage-specific gene encoding a major matrix protein of the sea urchin embryo spicule. II. Structure of the gene and derived sequence of the protein. *Dev Biol* 120:507–519.
31. Katoh-Fukui Y, et al. (1991) The corrected structure of the SM50 spicule matrix protein of *Strongylocentrotus purpuratus*. *Dev Biol* 145:201–202.
32. Killian CE, Wilt FH (1996) Characterization of the proteins comprising the integral matrix of *Strongylocentrotus purpuratus* embryonic spicules. *J Biol Chem* 271:9150–9159.
33. Peled-Kamar M, Hamilton P, Wilt FH (2002) The spicule matrix protein LSM34 is essential for biomineralization of the sea urchin spicule. *Exp Cell Res* 272:56–61.
34. Metzler RA, et al. (2008) Probing the organic-mineral interface at the molecular level in model biominerals. *Langmuir* 24:2680–2687.
35. Metzler RA, et al. (2008) Polarization-dependent imaging contrast in abalone shells. *Phys Rev B* 77:064110.
36. Seto J, Zhang Y, Hamilton P, Wilt F (2004) The localization of occluded matrix proteins in calcareous spicules of sea urchin larvae. *J Struct Biol* 148:123–130.
37. Urry LA, Hamilton PC, Killian CE, Wilt FH (2000) Expression of spicule matrix proteins in the sea urchin embryo during normal and experimentally altered spiculogenesis. *Dev Biol* 225:201–213.
38. Levi-Kalisman Y, Raz S, Weiner S, Addadi L, Sagi I (2000) X-Ray absorption spectroscopy studies on the structure of a biogenic "amorphous" calcium carbonate phase. *J Chem Soc Dalton Trans* 3977–3982.
39. Suzuki M, et al. (2009) An acidic matrix protein, Pif, is a key macromolecule for nacre formation. *Science* 325:1388–1390.
40. Söllner C, et al. (2003) Control of crystal size and lattice formation by starmaker in otolith biomineralization. *Science* 302:282–286.
41. Politi Y, Arad T, Klein E, Weiner S, Addadi L (2004) Sea urchin spine calcite forms via a transient amorphous calcium carbonate phase. *Science* 306:1161–1164.
42. Weiss IM, Tuross N, Addadi L, Weiner S (2002) Mollusc larval shell formation: Amorphous calcium carbonate is a precursor phase for aragonite. *J Exp Zool* 293:478–491.
43. Marxen JC, Becker W, Finke D, Hasse B, Epple M (2003) Early mineralization in *Biomphalaria glabrata*: Microscopic and structural results. *J Mollus Stud* 69:113–121.
44. Bentov S, Weil S, Glazer L, Sagi A, Berman A (2010) Stabilization of amorphous calcium carbonate by phosphate rich organic matrix proteins and by single phosphoamino acids. *J Struct Biol* 171:207–215.
45. Vinogradov AP (1953) *The Elementary Chemical Composition of Marine Organisms.* (Yale Univ Press, New Haven, CT).
46. Dillaman R, Hequembourg S, Gay M (2005) Early pattern of calcification in the dorsal carapace of the blue crab, *Callinectes sapidus*. *J Morphol* 263:356–374.
47. Neues F, Ziegler A, Epple M (2007) The composition of the mineralized cuticle in marine and terrestrial isopods: A comparative study. *CrystEngComm* 9:1245–1251.
48. Raz S, Testeniere O, Hecker A, Weiner S, Luquet G (2002) Stable amorphous calcium carbonate is the main component of the calcium storage structures of the crustacean *Orchestia cavimana*. *Biol Bull* 203:269–274.

49. Becker A, et al. (2003) Structural characterisation of X-ray amorphous calcium carbonate (ACC) in sternal deposits of the crustacea *Porcellio scaber*. *Dalton Trans* 4:551–555.
50. Becker A, Ziegler A, Epple M (2005) The mineral phase in the cuticles of two species of Crustacea consists of magnesium calcite, amorphous calcium carbonate, and amorphous calcium phosphate. *Dalton Trans* 10:1814–1820.
51. Chave KE (1954) Aspects of the biogeochemistry of magnesium I. Calcareous marine organisms. *J Geol* 62:266–283.
52. Darwin C (1881) *The Formation of Vegetable Mould, Through the Action of Worms, with Observations on Their Habits* (John Murray, London).
53. Gago-Duport I, Briones MJ, Rodriguez JB, Covelo B (2008) Amorphous calcium carbonate biomineralization in the earthworm's calciferous gland: Pathways to the formation of crystalline phases. *J Struct Biol* 162:422–435.
54. Lee MR, Hodson ME, Langworthy G (2008) Earthworms produce granules of intricately zoned calcite. *Geology* 36:943–946.
55. Sethmann I, Worheide G (2008) Structure and composition of calcareous sponge spicules: A review and comparison to structurally related biominerals. *Micron* 39:209–228.
56. Lambert G, Lambert CC, Lowenstam HA (1990) *Skeletal Biomineralization: Patterns, Processes and Evolutionary Trends*, ed JG Carter (Van Nostrand Reinhold, New York), Vol 1, pp 461–469.
57. Mahamid J, Sharir A, Addadi L, Weiner S (2008) Amorphous calcium phosphate is a major component of the forming fin bones of zebrafish: Indications for an amorphous precursor phase. *Proc Natl Acad Sci USA* 105:12748–12753.
58. Beniash E, Metzler RA, Lam RSK, Gilbert PUPA (2009) Transient amorphous calcium phosphate in forming enamel. *J Struct Biol* 166:133–143.
59. Gilbert PUPA, Haeberli W (2011) *Physics in the Arts, Revised Edition* (Elsevier-Academic, Burlington, MA).
60. Frazer BH, Girasole M, Wiese LM, Franz T, De Stasio G (2004) Spectromicroscope for the photoelectron imaging of nanostructures with X-rays (SPHINX): Performance in biology, medicine and geology. *Ultramicroscopy* 99:87–94.